Subpicosecond study of carrier trapping dynamics in wide-band-gap crystals

P. Martin, S. Guizard, Ph. Daguzan, and G. Petite
Service de Recherche sur les Surfaces et l'Irradiation de la Matière, Commissariat à l'Energie Atomique, DSM/DRECAM, CEN Saclay, 91191 Gif sur Yvette, France

P. D'Oliveira, P. Meynadier, and M. Perdrix
Service des Photons, Atomes et Molécules, Commissariat á l'Energie Atomique, DSM/DRECAM, CEN Saclay, 91191 Gif sur Yvette, France

(Received 3 October 1996)

Using a very sensitive time-resolved interferometric technique, we study the laser induced carrier trapping dynamics in wide band-gap crystals with 100 fs temporal resolution. The fast trapping of electrons in the band-gap is associated with the formation of self-trapped excitons (STE's). The STE's formation kinetics does not depend on the pump laser intensity in SiO_2, while the trapping rate increases in NaCl with the excitation density. We interpret this result as a direct evidence of exciton trapping in the first case, and an electronic trapping following a hole trapping in the second. This result is explained in terms of electron trajectories calculated with a simple Monte Carlo simulation: the electrons can explore a large volume before being trapped in NaCl, not in SiO_2. A temperature influence on the initial trapping process is observed in KBr, not in NaCl and SiO_2. Finally, we find no evidence of STE formation in diamond. This result is in agreement with general consideration about the STE's formation in terms of lattice elasticity and deformation potentials. [S0163-1829(97)01110-7]

I. INTRODUCTION

When a lattice is not stable upon creation of electron-hole pairs, an electron, a hole, or a bound electron-hole pair (exciton) can be trapped in its own lattice deformation. This self-trapping process, occurring in materials where the coupling between carriers and phonons is strong, has received for a long time a considerable interest especially in wide band gap solids because it is supposed to be the initial step in defect creation mechanisms. The development of femtosecond laser pulses is very helpful to understand these phenomena because it is now possible to separate the different steps of the trapping process and then to perform studies of defects formation dynamics. Experiments are usually based on spectroscopic measurements: a first pulse (pump) creates electron-hole pairs whereas a second pulse (probe) is used to test the absorption coefficient of the perturbed material after a controlled time delay. Several time-resolved spectroscopic measurements have been performed in alkali halides such as NaCl,[1] KBr,[2] and in oxides such as SiO_2.[3,4] Recently, time-resolved experiments based on the concept of interferometry in the frequency domain have been performed.[5] This method is very powerful because it allows a direct observation of the modification of the dielectric function of the material due to the pump pulse, and thus, to measure the lifetime of photoexcited carriers. The evolution of the electronic excitation density has been studied in this way in three oxides (SiO_2, MgO, Al_2O_3).[6] While the lifetime of electrons in the conduction band is respectively 50 ps and 100 ps in MgO and Al_2O_3, a mean electron trapping time of 150 fs has been measured in quartz. This trapping time coincides with the rise time of the self-trapped-exciton (STE) absorption band, leading to the conclusion that the electronic trapping is associated with the formation of STE's.[4] In order to investigate the role of the sample ionicity in these phenomena, this interferometric technique has been applied to several other materials going from pure ionic solids (NaCl, KBr) to a pure covalent one (diamond) *via* a material presenting a mix ionocovalent character (SiO_2). The influence of the pump laser pulse intensity and sample temperature has been studied for two probe wavelengths: 790 and 618 nm.

The experimental results presented in this work can be understood with the help of some basic pictures proposed to explain the STE's formation some time ago, and constitute an experimental evidence for these models that are still not settled out of hand:[7] in quartz, STE's are formed from the electron and the hole of the same electron-hole pair, whereas in NaCl, their formation can be roughly interpreted as a two steps mechanism: first, a hole self-trapping occurs, and then an electron is captured by this hole, leading to an STE. Thus, the ultrafast carrier trapping is correlated to the STE formation. We will show that in KBr, contrary to NaCl, the sample temperature plays a role even in the initial trapping process. Our results are consistent with models which predict that STE's can exist in a given material, only if the lattice elasticity is large enough.[8]

In Sec. II, we describe the experimental setup and principle. In Sec. III, a phenomenological description of the excited material dielectric function is developed. The experimental data in SiO_2, NaCl, KBr, and diamond are presented in Sec. IV, as well as a kinetic model based on rate equations used to emphasize the difference of the STE's creation kinetics between SiO_2 and NaCl. The results of a Monte Carlo simulation of electron trajectories in NaCl and SiO_2, underlying the crucial role of the electron-phonon collisions, is presented in Sec. V. Finally, the elastic constants of the different materials studied here will be compared, and a correlation between elastic properties and radiation hardness will be pointed out.

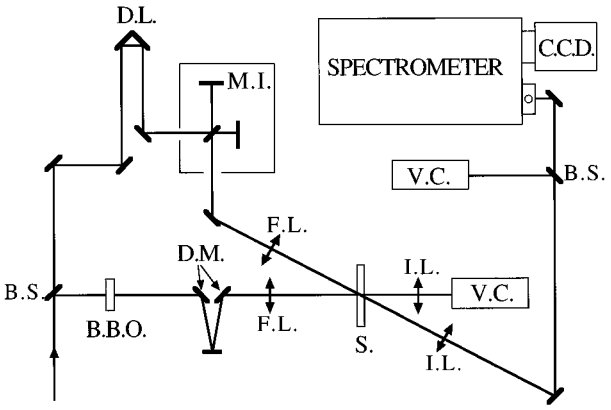

FIG. 1. Schematic representation of the experimental setup. BS: beam splitter, BBO: frequency doubling crystal, DL: delay line, MI: Michelson interferometer, DM: dichroic mirror, FL: focusing lens, S: sample, IL: imaging lens, VC: video camera, CCD: charge coupled device camera.

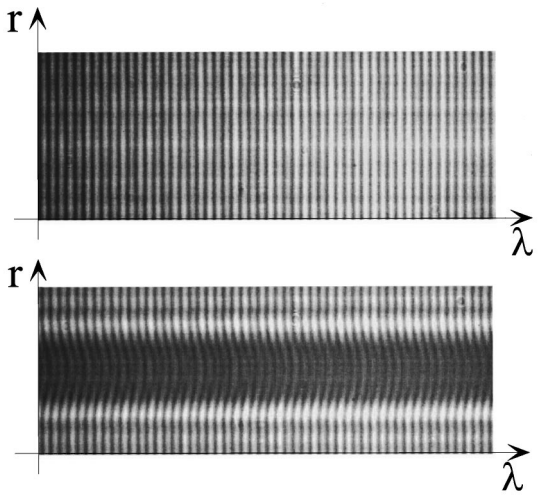

FIG. 2. Images of the two probe pulses spectrum obtained at the output of the spectrometer. Top: without pump pulse, bottom: a pump pulse has crossed the Al_2O_3 sample 3 ps before the second probe pulse. The vertical axis represents the distance from the center of the pump beam, and the horizontal axis the wavelength.

II. EXPERIMENTAL PRINCIPLE AND SETUP

The technique of interferometry in the frequency domain is a powerful and sensitive method to measure the phase shift occurring in the electric field of a probe laser pulse in the sample under study. This phase shift is obtained by analyzing the pattern resulting from interferences between a probe and a reference beam, at the output of a spectrometer. This method was originally used to study the temporal transfer function of optical fibers.[9] The fiber was placed in one arm of a Mach-Zehnder-type interferometer, and the spectrum was obtained by scanning the wavelength of a tunable laser. The technique has been adapted for short laser pulses to measure the self-phase modulation occurring during the propagation in optical fibers.[10] In this case the spectrum is broad and no tunable source is needed. More recently, time resolved experiments using a pair of identical probe pulses separated by a fixed time delay have been performed. In this case, the sample is modified by a high intensity pump pulse, the reference and probe pulses impinging the sample respectively before and after the pump pulse.[11] Interferences between the two probe pulses can be observed if the grating of the spectrometer induces at the exit slit a temporal broadening larger than the delay between them. The advantage of this setup is to shake off the problem of the path difference between the two arms of a small Michelson interferometer and thus to remove the problem of the mechanic stability. Furthermore, since the optical paths are the same, the noise in the measured phase arising for instance from the roughness of the sample surface can be suppressed by comparing measurements with and without the pump pulse. This method was successfully used to study the dynamics of laser induced plasma at metal surfaces,[12] the refractive index modification of dielectric materials induced by a high intensity laser[5,6] and the oscillations of plasma density in the wake of an intense ultrashort laser pulse.[13]

In the present experiments, we used a mode-locked Ti:sapphire laser operating at a wavelength of 790 nm. The output of the oscillator is amplified in a regenerative amplifier, yielding 2 mJ, 120 fs pulses at a 20-Hz repetition rate. A block diagram of the experimental setup is drawn in Fig. 1. The first beam splitter reflects 90% of the main beam for the pump beam, whose frequency is doubled in a 500-μm-thick frequency doubling crystal (BBO). The fundamental and frequency doubled beams are separated by dichroic mirrors (DM). The coarse setting of the pump beam intensity is achieved by placing a circular aperture before the 300-mm focal lens that focuses the pump beam on the sample, and the fine adjustment obtained by changing the polarization of the beam at 790 nm with a half-wave plate located before the BBO crystal (not shown on Fig. 1). We used pulse energies at 395 nm in the range 2 to 22 μJ. The diameter (at $1/e$) of the pump beam is 34, 44, or 58 μm, yielding intensities between 2×10^{11} and 4×10^{12} W/cm^2. We used two probe wavelengths, 790 nm (the remaining 10% transmitted by the first beam splitter) or 618 nm. This wavelength is obtained by white light continuum generation in a water cell on which a part of the main Ti-Sapphire laser beam at 790 nm is focused. The white light pulse is amplified at 618 nm in three Rhodamine 6-G dye cells pumped by the second harmonic of a yttrium aluminum garnet (YAG) laser. The probe beam passes through a delay line (DL) and a small pinhole to improve the wave-front quality and increase the focal spot size. The two identical probe pulses are generated in a Michelson interferometer (MI); the delay between them is adjusted by translating one of the mirrors and was usually set at 12 or 18 ps. The interaction region is imaged on video cameras (VC) with lenses (IL) to ensure the alignment of pump and probe beams, and at the entrance slit of the spectrometer. A typical image observed at the output of the spectrometer and digitalized with a charge coupled device (CCD) camera is shown in Fig. 2: the horizontal axis is the wavelength, and the perpendicular axis is parallel to the slit of the spectrometer and therefore represents the vertical axis in real space. The spatial resolution is of the order of 1 μm. The interference pattern is clearly observed in this picture. Indeed, if one considers the electric field of the reference pulse $E_1(t)=E_0(t)e^{i\omega_0 t}$ and of the probe pulse, separated by a delay Δt: $E_2(t)=E_0(t-\Delta t)e^{i\omega_0(t-\Delta t)}$, the power spectrum of this sequence of two pulses is given by

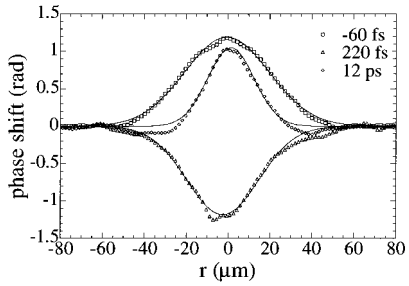

FIG. 3. Phase shift as a function of the distance from the center of the pump beam observed in NaCl for three different time delays between the pump and the second probe pulses.

$I(\omega)=2I_0(\omega)[1+\cos(\omega\Delta t)]$, leading to fringes in the spectrum separated by $2\pi/\Delta t$. In Fig. 2(b), a high intensity pump pulse crossed the sample (Al_2O_3 in this case) 3 ps before the passage of the second probe pulse. As a consequence, the refractive index experienced by the reference and probe pulses are slightly different. This induces a phase shift and a partial absorption, which readily manifest themselves in Fig. 2 (bottom) by a fringe pattern distortion and by a fringe contrast decrease, respectively. Let $\Delta\Phi$ be the phase shift and T the sample transmittance, the electric field of the second probe pulse is now $E_2(t)=\sqrt{T}E_0(t-\Delta t)e^{i[\omega_0(t-\Delta t)+\Delta\Phi]}$ and the spectrum of the interfering first and second probe pulses is given by $I(\omega)=I_0(\omega)\times[1+T+2\sqrt{T}\cos(\omega\Delta t+\Delta\Phi)]$. Since the perturbation depends on the pump laser intensity which has a Gaussian profile, the distortion of the fringes (the phase shift) and the fringe contrast (proportional to the transmittance) vary accordingly. If we suppose that the refractive index does not vary significantly during the probe pulse, a simple line by line Fourier transform of the image allows us to extract the desired informations: the phase shift and the transmittance (or absorption), as a function of a radial coordinate that represents the distance from the center of the pump beam. By repeating this operation for different time delays between the pump and the second probe pulse, we get the temporal evolution of these two quantities. As already emphasized, a dramatic signal to noise ratio improvement of the measured phase shift is obtained by comparing the phase obtained with and without pump pulse. The results are also averaged over three laser shots to limit the influence of shot to shot pump intensity fluctuations. Furthermore, the sample is displaced after each pump laser shot to work on a fresh area and avoid cumulative effects. We used in this experiment commercially available high purity (impurity content $\lesssim 1$ ppm), 500-μm thick and optically polished samples. The experiment sensitivity for the phase shift is 2×10^{-2} rad and the absorption coefficient is measured with a confidence of $\pm 5\%$.

In Fig. 3, the space-dependent phase shift for three time delays observed in NaCl at room temperature are presented. The pump intensity is 1,6 TW/cm^2 and the probe wavelength is 618 nm. Let us anticipate the discussion in Sec. III and qualitatively explain these three curves. The phase shift is proportional to the modification of the refractive index: $\Delta\Phi(r,t)=2\pi L/\lambda\times\Delta n(r,t)$, where r is the distance from the center of the pump beam, t the time elapsed since the crossing of the pump pulse, L is the length over which the probe and pump beams are overlapped in the sample (≈ 300 μm in the present experiments) and λ the probe wavelength. The zero time delay is defined as the coincidence of the maxima of the pump and second probe pulses. A delay -60 fs means that the refractive index of the material is probed 60 fs *before* the maximum of the pump pulse. In that situation, the pump and the second probe pulse are already temporally overlapped and we observe a positive phase shift which is due to the Kerr effect and is therefore proportional to the pump laser intensity. Each curve has a Gaussian profile as associated fits (full lines) show, and the full width at $1/e$, 56 μm, is thus in this case the size of the focused pump beam. For the delay $+220$ fs, probe and pump pulses no longer overlap and the signal is negative. This negative phase shift is proportional to the density of electrons in the conduction band. Finally, for longer time delays, the phase shift is positive and significantly narrower (32 μm) than the initial positive one. In this case the positive phase shift is proportional to the density of trapped electrons. Valence electrons must absorb three pump photons ($\hbar\omega_p=3.14$ eV) to bridge the 8.7 eV band-gap in NaCl. The density of trapped electron is thus proportional to the third power of the pump laser intensity. This explains the narrowing of the spatial distribution of trapped electron compared to the beam intensity profile. The spatial width ratio is almost exactly $\sqrt{3}$, the ratio expected for a three photon process. Finally the spatial resolution is very useful in two tasks: measuring the pump laser intensity *in situ*, which is inversely proportional to the pump beam surface, and checking the order of the multiphoton process at work in the excitation from the valence band to the conduction band.

III. REFRACTIVE INDEX MODEL

To interpret our experimental results, we need a model which describes the refractive index ''seen'' by the first probe pulse and the second one after the pump pulse. In the following equations, only the electronic contribution to the dielectric function is taken into account. We consider that the first pulse interacts with the wide band-gap insulator in its fundamental state and we represent the medium with a population of two level systems. In that case, the dielectric function reads

$$\epsilon_1(\omega)=1+\frac{N_0e^2}{m\varepsilon_0}\frac{f_{12}}{\omega_{12}^2-\omega^2-i\omega/\tau_{12}}. \qquad (1)$$

N_0 is the valence electronic density, m the electron mass, ε_0 the vacuum permittivity, ω the probe pulsation, f_{12} the oscillator strength between the valence band (VB) and the conduction band (CB), ω_{12} stands for the energy difference between the VB and CB and $1/\tau_{12}$ is the width of the transition. Note that the dielectric function should include a summation over all possible transitions, f_{12} and ω_{12} must be considered in this expression as effective parameters representing this set of transitions. Anyway for our probe wavelengths, the samples used in the present work are quite transparent. We are indeed far from resonance ($\omega_{12}\approx 9$ eV$\gg\omega\approx 2$ eV) and the damping term (ω/τ_{12}) responsible for linear absorption can be neglected. In this case this expression is real and is nothing but the square of the usual

refractive index n_0, and we will use this value for the first (reference) probe pulse in all cases.

We consider now that the second probe pulse ''sees'' three different electronic populations: a density N_{CB} of electrons in the CB, a density N_{tr} of electrons trapped somewhere in the band-gap, and, of course, $N_0-N_{bc}-N_{tr}$ electrons still in the ground state. Furthermore, while the pump pulse is present in the medium, it contributes to the dielectric function by inducing a nonlinear polarization known as Kerr effect.[14] In this context, the dielectric function can be written as

$$\epsilon_2(\omega)=1+\frac{e^2}{m\varepsilon_0}(N_0-N_{CB}-N_{tr})f_{12}\frac{1}{\omega_{12}^2-\omega^2-i\omega/\tau_{12}}\frac{e^2}{\varepsilon_0}\times\left(-\frac{N_{CB}f_{CB}}{m^*}\frac{1}{\omega^2+i\omega/\tau_{e-p}}+\frac{N_{tr}f_{tr}}{m}\frac{1}{\omega_{tr}^2-\omega^2-i\omega/\tau_{tr}}\right)+\chi_{eff}^3E_p^2. \quad (2)$$

m^* is the electron effective mass in the conduction band, ω_{tr} is the energy difference between the fundamental and the first excited state of the induced defect, $1/\tau_{tr}$ the width of this transition, and f_{tr} is its corresponding oscillator strength. f_{CB} is the oscillator strength standing for the transitions occurring in the CB and $1/\tau_{e-p}$ simulates the electron-phonon collisions in the CB. χ_{eff}^3 is an effective third order nonlinear susceptibility and E_p the electric field associated with the pump laser pulse. Note that holes in the valence band or trapped in the band gap should contribute to the dielectric function in a similar way. The corresponding terms have been neglected in Eq. (2) because the effective masses of holes are much larger than that of electrons in the materials under study, except in diamond. It is important to underline that this hypothesis is not valid if the probe frequency matches a trapped hole transition since such a resonant behavior can offset the mass ratio. However, this is not the situation prevailing in the materials studied here: in NaCl and KBr, the optical absorption bands for holes (STE or for H center) lie in the range 3–4 eV, while those for the electron component are in the range of the probe wavelength used in the present experiments.[15] In the case of SiO_2, both electron and hole absorption bands are peaked above 4 eV, far from our probe photon energies.[16,17] This situation reinforce the argument of neglecting holes. Finally, let us emphasize that this simplification has in all cases little influence in our conclusion, except may be in the estimation of the excitation density.

In this model, the optical absorption spectra associated with electrons trapped in the band gap are represented by single absorption lines. In other words, f_{tr} must also be considered as an adjustable effective parameter because, at least in principle, several transitions with different probabilities are possible. Practically, we will consider in each case only the dominant term, i.e., the one which is the closest to resonant transitions for our probe wavelengths.

The phase shift and the induced absorption coefficient can easily be obtained from the above discussed definitions:

$$\Delta\Phi=\frac{2\pi}{\lambda}L[\mathrm{Re}(\varepsilon_2^{1/2})-\mathrm{Re}(\varepsilon_1^{1/2})], \quad (3)$$

$$A=1-\exp\left(-\frac{2L\omega}{c}\mathrm{Im}(\varepsilon_2^{1/2})\right]. \quad (4)$$

L is the length over which the pump and probe beams are superposed in the sample, and $\lambda=2\pi c/\omega$ is the probe wavelength.

In the fitting procedure that will be presented in the next section, Eqs. (2)–(4) have been used *in extenso*. But for the sake of clarity, let us assume that the density of excited electrons is small compared to the density of electrons in the fundamental state ($N_0\gg N_{CB},N_{tr}$) and that the damping terms can be neglected. The latter hypothesis is rough, but the former is valid since, as we shall see later, the excitation density in our experiments never exceeds 10^{19} cm^{-3}. With these approximations, a first order expansion of Eq. (2) replaced in Eq. (3) gives

$$\Delta\Phi=\frac{2\pi}{\lambda}L\left[n_2I_p+\frac{e^2}{2n_0\varepsilon_0}\left\{-\frac{N_{CB}f_{CB}}{m^*\omega^2}+\frac{N_{tr}f_{tr}}{m(\omega_{tr}^2-\omega^2)}\right\}\right]. \quad (5)$$

Although a crude estimate, this expression gives a good order of magnitude of the observed phase shifts[5,6] and is more convenient to identify the contribution of each term.

The first term represents the Kerr effect. It is proportional to the intensity of the pump laser I_p and contributes *positively* to the phase shift because at our probe wavelengths the nonlinear index (n_2) is positive. It is observed in all materials and will last as long as the pump and the probe pulses overlap in the sample. The second term, which is proportional to the density of electrons that have been excited by the pump pulse in the conduction band, is always *negative*. The last term stands for the trapping of the electrons subsequent to a defect formation. Its sign is determined by the relative values of ω_{tr} and ω. For example, in the case of shallow traps ($\omega_{tr}<\omega$), its contribution is *negative*. This means that the phase shift measurement alone is insufficient to distinguish the electrons in the conduction band and the electrons in shallow traps. On the contrary, if the absorption bands associated with the trapped state correspond to wavelengths shorter than the probe wavelength ($\omega_{tr}>\omega$), the trapping of electrons is revealed by the observation of a *positive* phase shift.

The absorption cross section is given by: $\sigma=2\omega\ \mathrm{Im}[\varepsilon_2^{1/2}]/cN$, where N stands for N_{CB} or N_{tr}. Taking into account the damping terms but supposing a ''low'' excitation density we get the following expression for σ:

$$\sigma=\frac{e^2}{n_0c\varepsilon_0}\left(\frac{f_{CB}/\tau_{e-p}}{m^*(\omega^2+1/\tau_{e-p}^2)}+\frac{f_{tr}\omega^2/\tau_{tr}}{m[(\omega_{tr}^2-\omega^2)+\omega^2/\tau_{tr}^2]}\right). \quad (6)$$

This probe photon absorption cross section includes the contribution of electrons in the conduction band (first part) and trapped in the band gap (second part). The first term arises from electron-photon-phonon collisions. It is responsible for laser heating of the electrons in the conduction band[18,19] and increases with the probe wavelength.

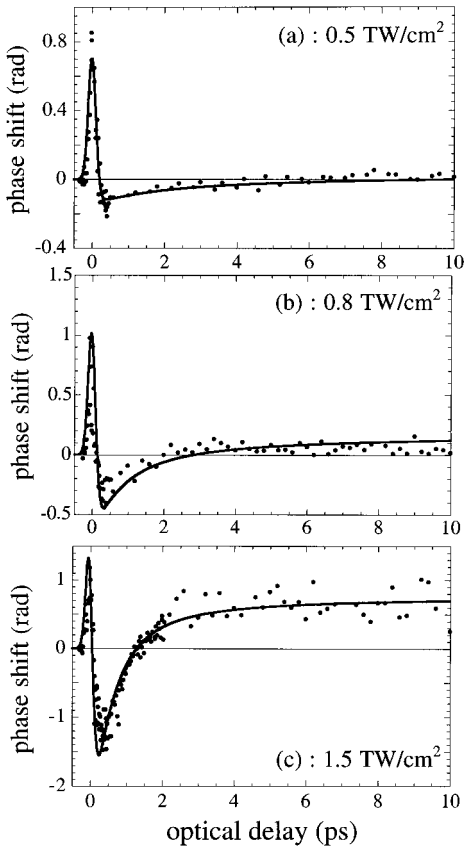

FIG. 4. Phase shift as a function of time measured in NaCl for three pump laser intensities. The probe wavelength is 618 nm and the sample is at room temperature.

IV. EXPERIMENTAL RESULTS AND KINETICS MODELIZATION

We now present and quantitatively discuss in detail the results obtained for different materials: NaCl, SiO_2, KBr, and C (diamond). Each point in the curves showing the temporal evolution of the measured phase shifts (and absorption) is obtained by spatially averaging the original data as those presented in Fig. 3. In the fitting procedure presented below, we consider the real experimental geometry: a Gaussian profile for the pump beam crossed by the probe beam at an angle of 10°. This means that for each time delay, Eqs. (3) and (4) are integrated along the path of the probe beam for each value of r (Fig. 3). This allows to take into account the spatial distribution specific for the Kerr effect and for the electron in the conduction band or trapped in the band gap.

Equations (3) and (4) are time-dependent because the electron populations N_{CB} and N_{tr} are time dependent. The kinetics of these populations can be simulated by using a set of rate equations. The basic idea is to postulate a time dependence for the trapping process, to solve numerically the set of rate equations and then to check if the results of Eqs. (3) and (4) fit the experimental data. The results of such simulations are presented in this section for NaCl and SiO_2 because their comparison shows a strikingly different behavior.

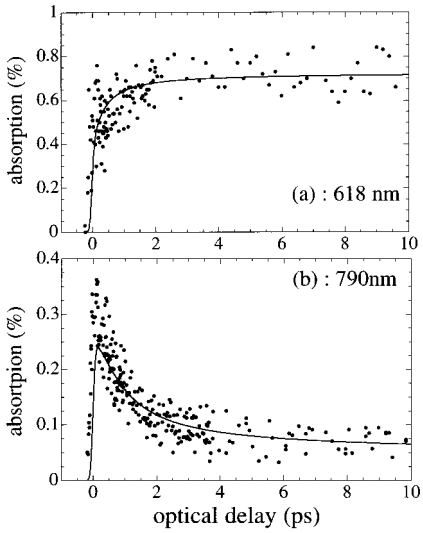

FIG. 5. Absorption as a function of time measured in NaCl for two pump laser wavelengths: 618 nm (a) and 790 nm (b).

A. The NaCl case

We show in Figs. 4(a)–4(c) the space integrated phase shift for NaCl for various pump intensities ranging from 0.5 to 1.5 T W/cm^2. The probe frequency is 618 nm and the sample is at room temperature. As already mentioned, we observe in all cases a positive phase shift for delays close to zero due to the Kerr effect. This gives us the temporal response of the pump-probe system, which is about 150 fs. At the end of the pump pulse, the phase shift becomes abruptly negative, due to the presence of electrons photoexcited in the conduction band. The most remarkable feature in NaCl is that the subsequent behavior of the signal depends on the pump laser intensity. In the low intensity limit [Fig. 4(a)], the signal goes back slowly to zero and becomes slightly positive for a delay equal to 5 ps. For a medium intensity [Fig. 4(b)], the phase shift becomes positive for 2 ps delay. In the highest intensity case [Fig. 4(c)], the phase shift reaches a positive value greater than in the above case but the time delay is now only 1.3 ps. Keeping in mind that the negative phase shift is proportional to the density of electrons in the conduction band and that the onset of a positive phase shift is the signature of a trapping process, we conclude from these observations that the *trapping kinetic is intensity dependent.* In other words, *the higher the excitation density, the faster the trapping process.*

Absorption measurements are very helpful to identify the nature of the trap. We show in Figs. 5(a) and 5(b), the absorption as a function of time obtained for comparable pump intensities (1.47 and 0.95 T W/cm^2) but for two different probe wavelengths: 618 and 790 nm. In both cases, a strong absorption peak is present at short times but for longer time delays, a constant absorption close to 70% is reached in the 618-nm case whereas this coefficient falls down to less than 10% at 790 nm. These experiments have been performed for two sample temperatures: 300 and 10 K. We did not remark any significant temperature dependence in the behavior of the phase shift and of the absorption coefficient for both probe wavelengths. This indicates that at the time scale of our experiment, i.e., up to 10 ps, the trapping center is the same at 10 K and at room temperature. Transient absorption spectra following electron pulse or picosecond laser excitation in NaCl at low temperature have been pub-

lished.[15,20] These spectra are attributed to the presence of STE's and exhibit a strong absorption band around 2.1 eV ($\approx$600 nm). We can therefore conclude that the trapping process at work in our experiment is the formation of STE's.

We now have to write rate equations describing the temporal evolution of the electron density in the conduction band N_{CB} and in trap levels N_{tr}. The observed trapping rate increases with the excitation density. This suggests a bimolecular-type kinetics, an hypothesis already formulated in alkali halides.[21,22] This suggests also that STE's are formed in a two-steps process: a hole trapping and then an electron trapping on a self-trapped hole (STH) site. In the corresponding rate equations, this two steps trapping process is described as follows: the hole trapping probability is simply an intrinsic trapping rate τ_h, a quantity which is believed to be less than a few ps (Ref. 8) but has not been yet precisely measured, while the trapping probability for an electron is proportional to the density of trapped holes (N_{th}) which are not yet occupied by an electron ($N_{th}-N_{tr}$).

These equations contain the populations of free and trapped holes, noted N_{fh} and N_{th}, respectively, and a source term that describes the creation of electron-hole pairs. As already pointed out, in NaCl this is a three photon excitation process. Finally the rate equations can be written as

$$
\begin{aligned}
&(d/dt)N_{CB}=\sigma^{(3)}F_p^3N_0-\sigma^{\text{capture}}vN_{CB}(N_{th}-N_{tr}),\\
&(d/dt)N_{tr}=\sigma^{\text{capture}}vN_{CB}(N_{th}-N_{tr}),\\
&(d/dt)N_{fh}=\sigma^{(3)}F_p^3N_0-N_{fh}/\tau_h,\\
&(d/dt)\,N_{th}=N_{fh}/\tau_h\,. \qquad (7)
\end{aligned}
$$

$\sigma^{(3)}$ is a generalized cross section for a three photon excitation process and F_p is the photon flux of the pump pulse. We take for N_0 the density of Cl atoms. The electron trapping rate is proportional to the product $\sigma^{\text{capture}}v$. The mean electron velocity in the CB v is chosen so that the electron kinetic energy corresponds to the energy of a LO phonon, which is roughly the electron energy after the relaxation in the CB.[15,23] σ^{capture} is the cross section for electron capture by a self-trapped hole. This quantity has been previously estimated to lie in the range of a few 10^{-14} cm^2.[21,24]

The electron-phonon coupling in NaCl is known to be less efficient than in SiO_2 as we will discuss in the next section. To perform the simulation, we took $\tau_{e-p}=10^{-15}$ s. The position of the maximum of the absorption band (ω_{tr}) and its associated width (τ_{tr}) are taken from the STE's absorption spectrum in NaCl[15]. The corresponding values are respectively 2.1 and 0.35 eV. In Table I, we present a summary of the set of parameters that fits satisfactorily the measured phase shifts for three pump laser intensities and the absorption for the two probe wavelengths (full lines in Figs. 4 and 5).

Given the relatively important number of adjustable parameters (n_2, $\sigma^{(3)}$, τ_{e-p}, f_{tr}, τ_{hole}, σ^{capture}), we do not claim that the set of parameters used in the simulation has a unique character. A satisfying fit of the five curves cannot, however, be obtained with significantly different values. On the other hand, it is evident from the data that the trapping kinetics cannot be described by a simple exponential law. But an important point to notice is that it is neither possible to fit the phase shift evolution for the three intensities without the assumption of a preliminary hole trapping. If we assume an instantaneous hole trapping, the electron trapping rate, initially proportional to the square of the excitation density, should indefinitely increase with increasing pump laser intensity. However, we observe experimentally that above excitation densities of the order of 10^{19} cm^{-3}, the delay for which the phase shift becomes positive is always the same ($\simeq$1.3 ps). This saturation of the trapping rate unambiguously demonstrates that the hole must first be self-trapped: at very high excitation densities, the electron trapping immediately follows the hole trapping, and the hole trapping rate ($\tau_{hole}=0.5$ ps) is readily measured from the high intensity data.

TABLE I. Set of parameters used in the simulation for NaCl.

Nonlinear refractive index (cm^2/W)	n_2	7×10^{-16}
initial valence electron density (cm^{-3})	N_0	2.24×10^{22}
order of the multiphoton process	n	3
Multiphoton cross section (cm^6 s^{-2})	$\sigma^{(3)}$	2×10^{-82}
Oscillator strength for the CB	f_{CB}	1
Electron-phonon scattering rate (s^{-1})	$1/\tau_{e-p}$	6×10^{14}
Electron effective mass in the CB (kg)	m^*	$0.5\times9.1\times10^{-31}$
Hole trapping time (ps)	τ_{hole}	0.5
Electron-hole capture cross section (cm^2)	σ^{capture}	8×10^{-14}
mean electron velocity in the CB (cm s^{-1})	ν	1.45×10^7
STE absorption band maximum (eV)	ω_{tr}	2.1
STE absorption band width (eV)	$1/\tau_{tr}$	0.35
Oscillator strength for the trap level	f_{tr}	0.25

We can also deduce from this simulation (from the maximum value of the negative phase shift) the electronic density achieved in the CB. For $I_p=1{,}5$ TW/cm^2 we obtain $N_{CB}\approx8\times10^{18}$ cm^{-3} and for $I_p=0{,}5$ TW/cm^2, $N_{CB}\approx4\times10^{17}$ cm^{-3}.

B. The SiO_2 case

In Figs. 6(a) and 6(b) the phase shifts measured at 618 nm at 300 K in a sample of Quartz (α-SiO_2) for two pump intensities, respectively 3 TW/cm^2 and 4 TW/cm^2 are shown. The order of the nonlinear process responsible for the injection of valence electrons in the CB has been measured with the method described above. We found a four photon absorption process in agreement with the fact that the band-gap in Quartz is equal to 10 eV (4×3.14 eV$\approx$12.5 eV). As a consequence, the initial excitation density is five times larger at 4 TW/cm^2 than at 3 TW/cm^2. As in the above case, we observe a positive phase shift due to the Kerr effect, immediately followed by a negative phase shift, which is proportional to the density of photoexcited electrons. As in NaCl, the evolution of the phase shift toward a positive value indicates a trapping of the electrons. However, contrary to the case of NaCl, the trapping kinetics is independent on the pump laser intensity. Although the initial excitation densities differ by a factor of 5, *the time necessary to get the positive phase shift (550 fs) is the same.* This behavior is, as in NaCl, independent of the sample temperature and of the probe

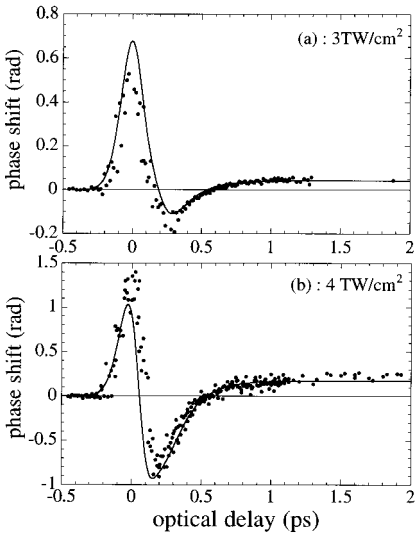

FIG. 6. Phase shift as a function of time measured in SiO_2 for two pump laser intensities. The probe wavelength is 618 nm and the sample temperature is 300 K.

wavelength. The absorption measured at 618 nm in the experimental conditions of Fig. 6(b) is shown in Fig. 7. We observe a decrease of the absorption while electrons are trapped in the band gap. This initial absorption is due to electron-phonon collisions. For longer time delays, it falls down to less than 10%, indicating that the probe photon energy is far from the resonances of the trapping center. The behavior of the phase shift and of the absorption is the same at 790 nm, and does not depend on the sample temperature.

It is now well known that ionizing radiations produce STE's in SiO_2.[25,26] The STE transient absorption band has maxima at 5.2 and 4.2 eV,[16,17] and it has recently been established from time-resolved absorption measurements that the rise time of the absorption peak at 5.2 eV coincides, within experimental errors, with the electron trapping time.[6] There are therefore no doubt that the trapping process in SiO_2 is due to the formation of STE's.

An intensity independent kinetics is the signature of a nonsequential or exponential trapping. Accordingly, the rate equations governing the density of trapped and conduction electrons simply include a multiphoton excitation source term and an exponential decay,

$$(d/dt)N_{\mathrm{CB}} = N_0\sigma^{(4)}F_p^4 - N_{\mathrm{CB}}/\tau,$$
$$(d/dt)N_{\mathrm{tr}} = N_{\mathrm{CB}}/\tau. \qquad (8)$$

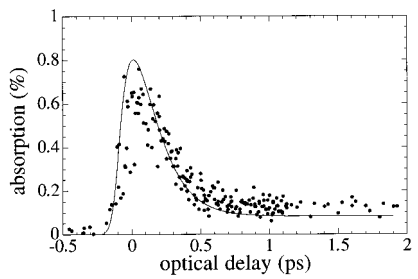

FIG. 7. Absorption as a function of time measured in SiO_2. The pump intensity is 1.5 T W/cm^2. The probe wavelength is 618 nm and the sample temperature is 300 K.

TABLE II. Set of parameters used in the simulation for SiO_2.

Nonlinear refractive index (cm^2/W)	n_2	2×10^{-16}
initial valence electron density	N_0	2.2×10^{22}
Order of the multiphoton process	n	4
Multiphoton cross section (cm^{8}s^{-3})	$\sigma^{(4)}$	2.3×10^{-114}
Oscillator strength for the CB	f_{cb}	1
Electron effective mass in the CB (kg)	m^*	$0.5\times9.1\times10^{-31}$
Electron-phonon scattering rate (s^{-1})	$1/\tau_{e-p}$	1.5×10^{15}
Electron trapping time (fs)	τ	150
Oscillator strength for the trap level	f_{tr}	0.4 and 0.15
Trap level energy (eV)	ω_{tr}	$5.2 and 4.2$
Width of the trap level (eV)	$1/\tau_{\mathrm{tr}}$	1.5 and 1

The parameters for which Eqs. (3), (4), and (8) give the best fit of the experimental results are summarized in Table II. The parameters ω_{tr} and τ_{tr} are taken from the published transient absorption spectra.[16]

The electron-phonon coupling is responsible for the electronic energy loss in the CB and is taken as 1.5×10^{15} s^{-1}. As already pointed out, this term is also responsible for photon absorption while electrons are in the conduction band.

For small positive delays, say 0 to 200 fs, the phase shift dramatically varies from a positive value due to the Kerr effect, to a negative value while electrons are excited in the conduction band. Therefore the assumption that the refractive index does not change significantly during the probe pulse is not valid in this situation. This is the origin of the slight disagreement in this temporal region. The agreement between experimental data and the curve fit is, however, quite good for longer time delays, leading to a strong confidence in exponential law assumed in the kinetic equations and in the decay time of 150 fs obtained from the fitting procedure. Finally the main conclusion is the simultaneous trapping of the hole and the electron: in quartz the trapping really concerns the *exciton*. Indeed, contrary to alkali halides, no hole trapping is observed in α-SiO_2 (Ref. 27) and according to *ab initio* Hartree-Fock calculation in SiO_2 clusters, the stabilization of the STE is due to the electron rather than to the hole.[28] Hole trapping has been suggested in amorphous silica (a-SiO_2),[29] but we have measured the same trapping kinetics[5] and the same absorption rise time[4] in a-SiO_2 than in α-SiO_2, indicating that the exciton trapping process is the same in both cases.

C. The KBr case

We present in Figs. 8 the phase shifts (top curves) and absorption (bottom curves) obtained in KBr with two probe wavelengths: 618 nm [Figs. 8(a) and 8(b)] and 790 nm [Figs. 8(c) and 8(d)], at two sample temperatures: 300 K [Figs. 8(a) and 8(c)] and 10 K [Figs. 8(b) and 8(d)]. The pump intensity is the same in all cases and is of the order of 1 T W/cm^2. The range of intensities that can be explored in KBr is much more limited than in other materials because, for higher intensities and especially at 618 nm, the absorption is so strong that it rapidly reaches 100%, making interference measurements impossible. In all cases, we observe a rapid evolution of the signal (phase shift and absorption) during the first 4 ps. In the limited accessible intensity range, we could not

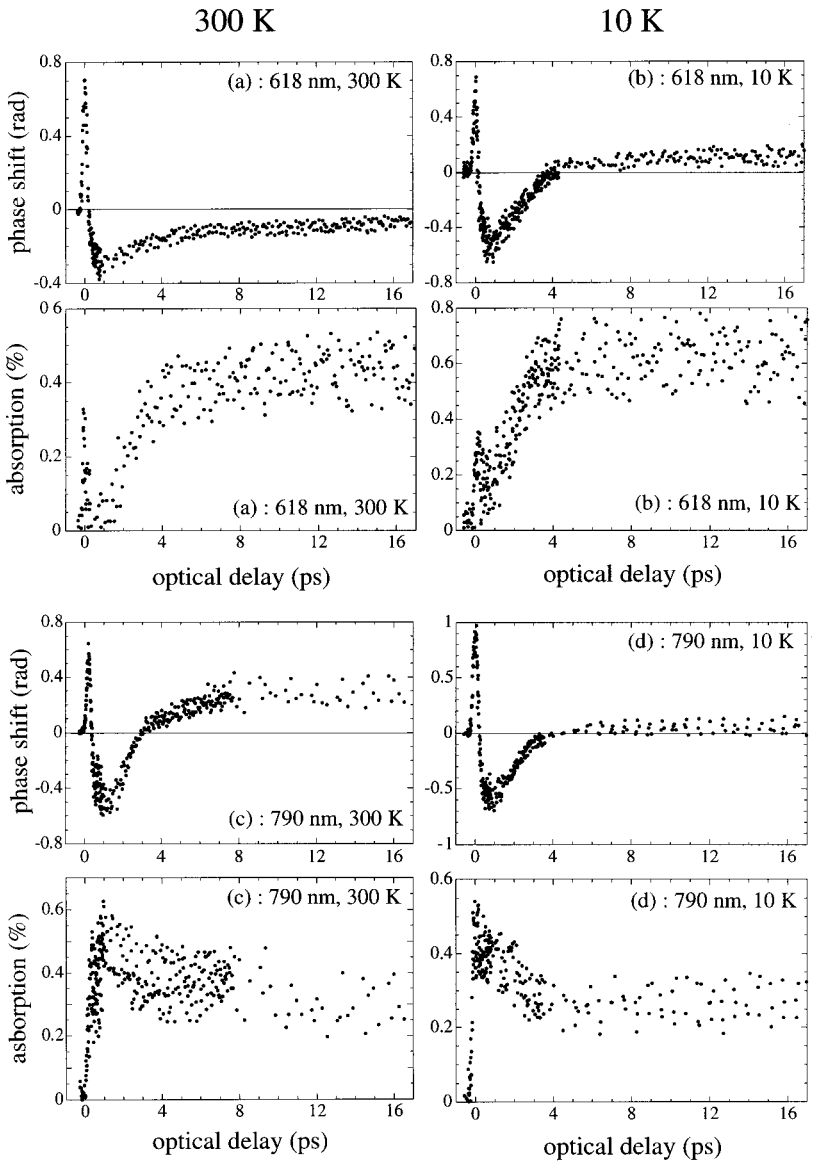

FIG. 8. Phase shift (top curves) and absorption (bottom curves) measured in KBr at 300 K [left column: (a),(c)] and 10 K [right column: (b),(d)] and at two probe wavelengths: 618 nm [top: (a),(b)] and 790 nm [bottom: (c),(d)]. The pump intensity is of the order of 7×10^{11} W/cm^2.

observe any excitation density influence on the kinetics as in NaCl. This last point is not consistent with previous free-electron lifetime measurements in KBr based on photoconductivity experiments.[22] It has been shown that when the excitation density is low, the electron lifetime is about 10–20 ns and the recombination process is due to extrinsic trapping. For increasing excitation density, intrinsic trapping following bimolecular kinetics is observed, but above 10^{17}/cm^3, the experimental resolution did not allow a precise determination of the lifetime, which becomes less than 10 ps. From the present high resolution results we could conclude that the trapping is not sequential but as we noticed in NaCl, above a given excitation density the trapping kinetics is limited by the hole trapping time, and we cannot exclude that the lowest excitation density ($\sim10^{18}$/cm^3) explored in KBr is already above this threshold.

The striking feature concerning the phase shift is that it becomes positive after 4$\sim$5 ps in all cases except at 300 K, 618 nm [Fig. 8(a), top curve]. According to our refractive index model, the conclusion of this observation is that electronic state associated with the trap in the band gap presents absorption bands peaked at energies lower than 2 eV at 300 K, and higher than 2 eV at 10 K. Of course the real situation can be more complicated than what our simple model describes. In particular it is possible that different states with different absorption bands are populated simultaneously: the phase shift in such cases gives an averaged measurement of these different populations. Indeed Alkali halides have been classified in two classes.[30] In type-I materials such as NaCl, the STE's recombine radiatively at low temperature and the formation of *F-H* pairs occurs via thermal activation along the lowest state of the STE. In this case the yield of STE luminescence and stable *F-H* pairs formation are anticorrelated. In KBr, which belongs to type-II alkali halides, *F-H* pairs are created even at low temperature and no such anticorrelation is observed. Recent time resolved absorption measurements have shown that the populations of STE's and *F* centers following electronic excitation evolve in two time scales:[2,7] a rapid evolution ($\tau\approx2$ ps) which we readily observe in our phase shift and absorption measurements, and a slower ($\tau\approx40$ ps), that we did not investigate in the present set of experiments. The ultrafast dynamical process leading to the formation of *F* centers is so efficient that the associated absorption band around 2 eV dominates the transient

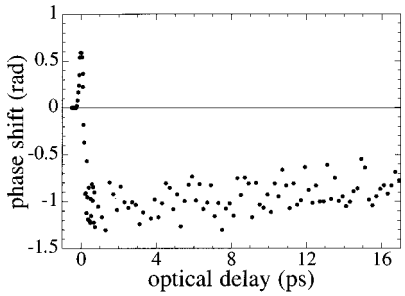

FIG. 9. Phase shift measured in diamond at 300 K. The probe wavelength is 618 nm and the pump intensity is 3×10^{11} W/cm^2.

absorption spectrum after only 3 ps.[2,7] The behavior of the phase shift after the first 3 ps is therefore controlled by the presence of F centers. This hypothesis is confirmed by our absorption data. The absorption at 618 nm mainly due to F centers, increases while the electrons are trapped. At 790 nm the initial absorption is due to the electrons in the conduction band and decreases to a value lower than at 618 nm. The remaining absorption is due to the STE's. Moreover, it has been established a long time ago[31] that the absorption spectrum of F centers in KBr is shifted towards low energy and broadened when the temperature increases: it is peaked at 600 nm (2.1 eV) at 73 K and at 630 nm (1.95 eV) at 300 K. In that case, it is not surprising that the phase shift is always positive at 790 nm and changes its sign at 618 nm when the temperature changes from 10 to 300 K.

D. The diamond case

In Fig. 9 the phase shift obtained for a pure diamond sample at 300 K (the pump intensity is 3×10^{11} W/cm^2) is shown for a probe wavelength of 618 nm. We observe that the phase shift is negative and remains constant. This behavior is identical at both probe wavelengths, whatever the pump intensity and the sample temperature. Even for intensities as high as 1.5 T W/cm^2 we were not able to see any modification in this behavior.

According to the experimental results, no trapping is visible in diamond. We conclude that, at such time scales, if the electrons are trapped, they are trapped into levels very close to the bottom of the conduction band.

Because no clear evidence of change in the phase shift appears during the time that separates the two probe pulses, we performed measurements in the relative mode: we let the two probe pulses cross the sample after the pump pulse. If we suppose an exponential decay (lifetime τ) of the electron density in the CB, the phase shift and absorption are in this case given by: $\Delta\Phi=\Delta\Phi_0(e^{[-t/\tau]}-e^{[-(t-\Delta t)\tau]})$ and $A=A_0(e^{(-t/\tau)}+e^{[-(t-\Delta t)\tau]})$, where $\Delta\Phi_0$ and A_0 are the phase shift and the absorption just after the pump pulse. This method is less sensitive than the absolute one but much longer time delays can be investigated. The result of relative measurements performed at room temperature in diamond are shown in Figs. 10(a) and 10(b). The pump wavelength and intensity are respectively 618 nm and 0.7 T W/cm^2. The fits give 140 and 190 ps as time decay for the phase shift and absorption, respectively. The latter value is certainly more reliable, due to the larger scattering in the absorption data.

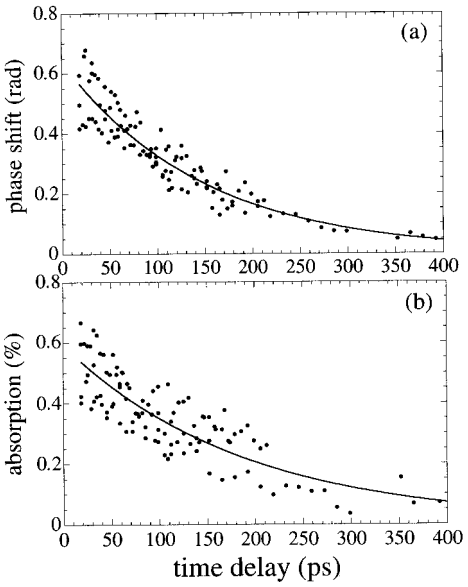

FIG. 10. Relative phase shift [top: (a)] and absorption [bottom: (b)] measured in diamond at 300 K. The probe wavelength is 618 nm and the pump intensity is 8×10^{11} W/cm^2.

V. ELECTRON TRANSPORT IN NaCl AND SiO_2: MONTE CARLO SIMULATION

The experimental results have revealed an important difference between SiO_2 and NaCl: the electron trapping time does not depend on the conduction electron density in SiO_2, while it is strongly dependent on carrier density in NaCl. This observation led us to describe the evolution of the electron density in the conduction band in NaCl with bimolecular kinetics. The same model has been used to interpret time resolved absorption experiments in alkali halides.[21] In NaCl, STE's consist of a hole, relaxed to the form of a Cl_2^- molecular ion and an electron. After the creation of an electron-hole pair by the incident radiation, the molecular ion formation results from the self-trapping of a hole in a very short time, estimated to be less than 1 ps;[7] then an electron is captured by a hole and a STE is formed. The underlying hypothesis in this two steps process is that electrons can explore a volume large enough to contain many STH's. In the case of SiO_2, the STE's creation rate is governed by an exponential law independent on the excitation density. Each electron-hole pair remains in interaction until the STE is formed. So the difference of behavior of the electron trapping time versus the pump intensity can be explained if the electrons can run away from their hole in NaCl and not in SiO_2.

Knowing exactly the minimum electron-hole distance necessary to prevent the trapping of an electron by a hole is a difficult task, but as a first approximation, one can use the simple following arguments. When an electron-hole pair is created by the pump pulse, there is a coulomb attraction between them until they get far apart. In order to estimate the distance necessary for the carriers to avoid recombination, one can take the distance (r_c) at which the Coulomb energy becomes equal to the thermal energy (3/2 kT). One finds $r_c(SiO_2)=97$ Å and $r_c(NaCl)=63$ Å for T=300 K. Thus, if the electron reaches r_c with an energy greater than 3/2 kT, one can consider very roughly that electron's capture by the

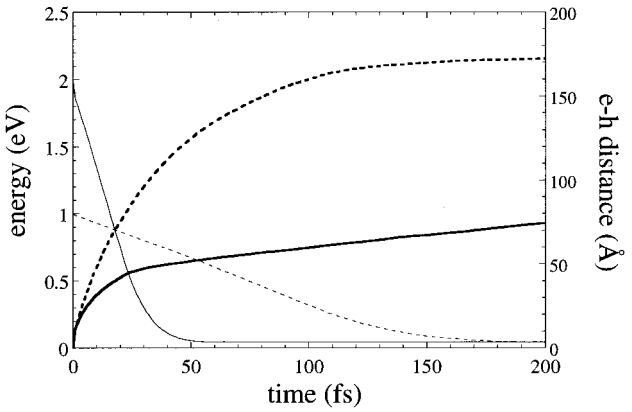

FIG. 11. Monte Carlo simulation of electron trajectories in SiO_2 (full lines) and NaCl (dashed lines). The light lines show the kinetic energy (left scale) and the heavy lines the electron-hole distance (right scale).

hole becomes impossible.[32] To evaluate the time dependence of the electron energy and the evolution of the electron-hole distance, we have performed a simple Monte Carlo simulation, based on the scheme developed by Fischetti *et al.*[33] The only interactions considered here are the LO and acoustical electron-phonon interactions, respectively treated with a Fröhlich Hamiltonian and a deformation potential approach. The hole is supposed not to move and there is no interaction between the electron and the hole. Electron transport in SiO_2 has been the subject of numerous study, and many physical data such as electron-phonon coupling constants are available.[33,23,34] In NaCl, these quantities seem to be known with a smaller precision, and especially electron-acoustical phonon coupling. According to several authors,[35,36] this interaction is smaller than in SiO_2. Electron-acoustical phonon collisions are isotropic, so they efficiently randomize the electron direction. Note that in order to take into account this lack of knowledge, we have tried different deformation potential values for NaCl, ranging from the value used for SiO_2 to this value divided by ten without noting significant changes in the results of the simulation. Electrons are injected in the CB with a kinetic energy ($nh\nu - E_g$) of 2 eV in SiO_2 and 1 eV in NaCl. The result of the Monte Carlo simulation is drawn in Fig. 11. We observe that electrons lose their energy much more quicker in SiO_2 than in NaCl, mainly due to the LO-phonon energy, larger in SiO_2 (150 meV) than in NaCl (30 meV). When the electron energy becomes of the order of thermal energy, the *e-h* distance is about 60 Å [$< r_c$ (SiO_2)] in SiO_2, whereas, this distance is about 150 Å [$> r_c$(NaCl)] in the case of NaCl. Consequently, we understand on the basis of this simple model that in NaCl an electron has a much greater chance to escape from its parent hole and meet another hole, whereas in SiO_2 an electron always remains in the vicinity of its hole and thus the STE formation involves the electron and the hole of the same initial pair. Let us underline that the interaction between electrons and holes is not taken into account in this model. However, the screening of the Coulomb potential is less efficient in quartz than in NaCl because the static dielectric constant is higher in the last case. Therefore, the inclusion of such an interaction should still enhance the relative pathways discussed above.

VI. CONCLUSIONS

The technique of interferometry in the frequency domain proved to be a very efficient and sensitive tool for the time resolved study of carriers excitation and relaxation dynamics in wide band gap insulators. Compared to for instance time resolved absorption spectroscopy, that brings fruitful information about the absorption bands associated with permanent (F and H centers) and transient states (STE, STH), the experiments reported in this paper provide complementary information. In particular, they offer the possibility to observe electrons in the conduction band and to measure with a good accuracy the excitation density. From this point of view, the absorption process due to electron-photon-phonon collision which occurs while electrons are in the conduction band is noteworthy. Its importance is evident before trapping in SiO_2 (Fig. 7) and increases for longer probe wavelengths, for example in NaCl at 790 nm [Fig. 5(b)], and also in a material where no trapping is observed [diamond, Fig. 10(b)].

Our experimental results demonstrate that the ultrafast trapping of carriers deep in the band gap observed in NaCl, KBr, and SiO_2, is in all cases associated with the formation of STE's. Furthermore, a detailed study of intensity dependence kinetics reveals two different pictures of STE's formation: hole trapping followed by electron capture in NaCl and exciton trapping in SiO_2. With the help of a simple Monte Carlo simulation, these different behaviors can be interpreted in terms of electrons trajectories: the electrons lose their energy quickly in SiO_2, while they have the possibility to move away from their own holes before being trapped in NaCl. The fitting procedure of the trapping kinetics allows us to extract for the first time the intrinsic hole trapping time in NaCl. Bimolecular kinetics are supposed to be a general rule in alkali halides, but are not observed in KBr, for excitation densities ranging over one decade from to 2×10^{17} to 2×10^{18} cm^{-3}. Electron capture is rather as fast as hole trapping or occurs simultaneously. Indeed it has been pointed out that different relaxation channels exist for electron hole pairs in KBr, depending on the time when the electron interacts with the hole under relaxation.[2]

The case of diamond is apparently very similar to the case of Al_2O_3 and MgO.[6] In these three materials, we do not observe evidence for STE's formation, but a slow decrease of the electron density in the conduction band with lifetimes lying in the range of 100 ps. It has been recently predicted that in diamond, it should be possible to observe self-trapping in the case of valence biexcitons.[37] The maximum density reached in the above experiment is of the order of 10^{19} cm^{-3} (it is difficult to increase this excitation density without making serious damages to the sample) and we did not observe this related effect. This can be due to the fact that the excitation density in still not high enough. In Al_2O_3, the transient volume change induced by high-energy electrons has been ascribed to the formation of STE's.[38] However, intrinsic recombination luminescence has been observed in Al_2O_3 at 7.3 eV,[39] with an excitation spectrum sharply peaked at the band edge (exciton resonance).[40] This means that the stoke shift associated with eventual STE would be of the order of 1 eV or less. As already pointed out, our method could possibly not distinguish electron in the

conduction band or trapped close to the bottom of the conduction band. The same type of electron-hole recombination luminescence has been observed in MgO, indicating even smaller stoke shifts.[41]

Among the properties that allow to predict the trend for exciton trapping in a given material, the ionicity certainly plays a role but is not a sufficient criteria to explain our results, since for instance STE's would be observed in MgO, much more ionic than SiO_2. As already mentioned, a STE is associated with a local deformation of the lattice around a bound electron-hole pair. This can be understood on the basis of simple and well-known scaling arguments. It is known that the consequence of the addition of an extra charge in a perfect lattice is to induce a relaxation of the lattice. The corresponding relaxation energy of the system is inversely proportional to the number of atomic bounds which support this extra charge (N_b) and then is minimum if $N_b=1$. In other words, the tendency of the system is to form a so-called ''small polaron.''[42] This energy which stabilizes the system is the sum of two terms coming from the electron-phonon interaction (acoustical and optical). On the other hand, this localization process has a cost. The latter is proportional to $1/N_b^{2/3}$ and the localization results from the competition between these two contributions. Toyozawa and co-workers[43] have located electrons, holes, and excitons in various solids into a phase diagram. One of the pertinent parameters to decide whether or not an exciton is self-trapped or free is the ratio C/ξ, where C is the deformation potential and ξ the elastic constant: the largest this ratio, the highest the self-trapping probability. So, self-trapping is favored in materials with high deformation potential and small elastic constant. In Table III the elastic constants relative to the materials which have been studied in this work are shown. It is clear that the elasticity plays a crucial role in the self-trapping process and that our data are in full agreement with the simple arguments discussed above.

TABLE III. Elastic constants in the (11) direction.

Material	C_{11} (GPa)	STE
C	1076	No
Al_2O_3	497	No?
MgO	294	No
SiO_2	87	Yes
NaCl	49	Yes
KBr	34	Yes

ACKNOWLEDGMENTS

Financial support from CEA-DAM is gratefully acknowledged.

[1] T. Tokizaki, T. Takimura, H. Akiyama, A. Nakamura, K. Tanimura, and N. Itoh, Phys. Rev. Lett. **67**, 2701 (1991).
[2] T. Shibata, S. Iwai, T. Tokisaki, K. Tanimura, A. Nakamura, and N. Itoh, Phys. Rev. B **49**, 13 255 (1994).
[3] P.N. Saeta and B.I. Greene, Phys. Rev. Lett. **70**, 3588 (1993).
[4] S. Guizard, P. Martin, G. Petite, P. D'Oliveira, and P. Meynadier, J. Phys. Condens. Matter **8**, 1281 (1996).
[5] P. Audebert, Ph. Daguzan, A. Dos Santos, J.C. Gautier, J.P. Geindre, S. Guizard, G. Hamoniaux, K. Krastev, P. Martin, G. Petite, and A. Antonetti, Phys. Rev. Lett. **73**, 1990 (1994).
[6] S. Guizard, P. Martin, Ph. Daguzan, and G. Petite, Europhys. Lett. **29**, 401 (1995).
[7] R.T. Williams and K.S. Song, J. Phys. Chem. Solids **51**, 679 (1990).
[8] K.S. Song and R.T. Williams, *Self-Trapped Excitons* (Springer-Verlag, Berlin, 1993).
[9] C. Froehly, A. Lacourt, and J.C. Vienot, J. Opt. (Paris) **4**, 183 (1973).
[10] F. Reynaud, F. Salin, and A. Barthelemy, Opt. Lett. **14**, 275 (1989).
[11] E. Tokunaga, A. Terasaki, and T. Kobayashi, Opt. Lett. **17**, 1131 (1992).
[12] J.P. Geindre, P. Audebert, A. Rousse, F. Falliès, J.C. Gautier, A. Mysyrowicz, A. Dos Santos, G. Hamoniaux, and A. Antonetti, Opt. Lett. **19**, 1997 (1994).
[13] J.R. Marquès *et al.*, Phys. Rev. Lett. **76**, 3566 (1996); C.W. Siders *et al.*, *ibid.* **76**, 3570 (1996).
[14] See for example, Y.R. Shen, *The Principals of Non-Linear Optics* (Wiley, New York, 1984).
[15] R.T. Williams and M.N. Kabler, Phys. Rev. B **9**, 1897 (1974).
[16] C. Itoh, K. Tanimura, and N. Itoh, J. Phys. C **21**, 4693 (1988).
[17] K. Tanimura, C. Itoh, and N. Itoh, J. Phys. C **21**, 1869 (1988).
[18] Ph. Daguzan, S. Guizard, K. Krastev, P. Martin, G. Petite, A. Dos Santos, and A. Antonetti, Phys. Rev. Lett. **73**, 2352 (1994).
[19] X.A. Shen, S.C. Jones, and P. Braunlich, Phys. Rev. Lett. **62**, 2711 (1989).
[20] R.T. Williams, B.B. Craig, and W.L. Faust, Phys. Rev. Lett. **52**, 1709 (1984).
[21] R.T. Williams, J.N. Bradford, and W.L. Faust, Phys. Rev B **18**, 7038 (1978).
[22] R.T. Williams, P.H. Klein, and C.L. Marquardt, in *Proceedings of the Conference on Laser Induced Damage in Optical Materials*, 1977, U.S. National Bureau of Standards Special Publication No. 509, edited by A.J. Glass and A.H. Guenther (U.S. GPO, Washington, D.C., 1978).
[23] Ph. Daguzan, P. Martin, S. Guizard, and G. Petite, Phys. Rev. B **52**, 17 099 (1995).
[24] S.C. Jones, A.H. Fischer, P. Braunlich, and P. Kelly, Phys. Rev. B **37**, 755 (1988).
[25] K. Tanimura, T. Tanaka, and N. Itoh, Phys. Rev. Lett. **51**, 423 (1983).
[26] W. Hayes, M.J. Kane, O. Salminen, R.L. Wood, and S.P. Doherty, J. Phys. C **17**, 2943 (1984).
[27] W. Hayes and T.J.L. Jenkins, J. Phys. C **19**, 6211 (1986).
[28] A.J. Fisher, W. Hayes, and A.M. Stoneham, J. Phys. Condens. Matter **2**, 6707 (1990).
[29] D.L. Griscom, Phys. Rev. B **40**, 4224 (1989).
[30] N. Itoh, T. Eshita, and R.T. Williams, Phys. Rev. B **34**, 4230 (1986).
[31] R.W. Pohl, Proc. Phys. Soc. **49**, 3 (1937).
[32] R.C. Hughes, Solid State Commun. **21**, 251 (1978).
[33] M.V. Fischetti, D.J. DiMaria, S.D. Brorson, T.N. Theis, and J.R.

Kirtley, Phys. Rev. B. **31**, 8124 (1985).
[34] D. Arnold, E. Cartier, and D.J. DiMaria, Phys. Rev. B **49**, 10 278 (1994).
[35] M. Sparks, D.L. Mills, R. Warren, T. Holstein, A.A. Maradudin, L.J. Sham, E. Loh, Jr., and D.F. King, Phys. Rev. B **24**, 3519 (1981).
[36] S.C. Jones, A.H. Fischer, P. Braunlich, and P. Kelly, Phys. Rev. B **37**, 755 (1988).
[37] F. Mauri and R. Car, Phys. Rev. Lett. **75**, 3166 (1995).
[38] C. Itoh, K. Tanimura, and N. Itoh, J. Phys. C **19**, 6887 (1986).
[39] W.A. Runciman, Solid State Commun. **6**, 537 (1968).
[40] V. Mürk, B. Namozov, and N. Yaroshevich, Radiat. Meas. **24**, 371 (1995).
[41] Z.A. Rachko and J.A. Valbis, Phys. Status Solidi **93**, 161 (1979); Y.A. Valbis, K.A. Kalder, I.L. Kuusmann, C.B. Lushchick, A.A. Ratas, Z.A. Rachko, M.E. Springis, and V.M. Tiit, JETP Lett. **22**, 36 (1975).
[42] W. Hayes and Stoneham, *Defects and Defect Processes in Nonmetallic Solids* (Wiley, New York, 1985).
[43] M. Ueta, H. Kanzaki, K. Kobayashi, Y. Toyozawa, and E. Hanamura, *Excitonic Processes in Solids* (Springer, Berlin, 1986).